17

Photovoltaic GaAs Detectors for Digital X-Ray Imaging

V.F. Dvoryankin, G.G. Dvoryankina, Yu.M. Dikaev, M.G. Ermakov, A.A. Kudryashov, A.G. Petrov and A.A. Telegin
Institute for Radio engineering and Electronics of Russian Academy of Sciences, Russia

1. Introduction

The short coming of the conventional film-screen systems arises from limited dynamic range due to the film latitude and Swank noise from the screen and film granularity that limits the system rather than quantum fluctuations. A thin intensifying screen is used to achieve better spatial resolution; however thin screens also have limited detector quantum efficiency. Most currently available digital X-ray systems use scanned-slit geometries to minimize tehe required detector area and minimize system complexity. Scanned-slit systems achieve also efficient rejection of Compton scattered X-rays by suffering significant X-ray tube loading in comparison to conventional large-field imaging geometries. There remains a significant clinical need in production of detection systems with sufficiently high spatial resolution and detection quantum efficiency. An improvement of digital radiography compared to conventional systems is the high dynamic range. Futhermore real-time data acquisition is possible and digital image processing can be performed. A digital image representation has become feasible because of the availability of digital mass storage media.

In the past years , considerable attention was paid to the fabrication of X-ray detectors based on LEC SI GaAs (Amendolia et al., 1999; Bates, 1998; Bencivelly, 1994), LPE GaAs (Alexiev & Butcher, 1992), LP VPE GaAs (Adams et al., 1997; Bates et al., 1998) and GaAs pin structures fabricated by combining LPE and VPE (Bates et al., 1999). Early bulk devices suffered from poor charge collection efficiency and intermittent burst noise and, while later devices fabricated by LPE, LP VPE and the combination of LPE and VPE epitaxial deposition techniques proved to be good detectors, they suffered from poor detector efficiency due to the difficulties in producing thick low-doped epitaxial layers. Two types of semiconductor devices are used usually: pin diodes (McGregor&Hermon, 1997) and Schottky diodes (Buttar, 1993) operating at reverse bias voltages. A rather high (1 – 2 V/μm) operating bias voltage leads to an increase of detector noise arising from the leakage currents.

In order to reduce that noise it is necessary to operate at low temperatures. We have developed a new photovoltaic X-ray detector based on an epitaxial p^+-n-n′-n^+ GaAs structure (Achmadullin, 2002) which ensures high performance without bias voltage at room temperature. The photovoltaic effect (i.e. the emergence of a photoelectromotive force) is observed in a semiconducting structure absorbing photons, which generate current

carriers (electron-hole pairs). These current carriers must be separated by the intrinsic electric field emerging in a heterogeneous semiconducting structure consisting of regions with different types of conductivity. There is some similarity between the X-ray detector and a solar cell based on GaAs (Jenny et al., 1956;Moizhes, 1960). But there is a difference too. The difference arises from higher operating energies of X-ray detector, that leads to the cecessity to solve more challenges. In the X-ray detector developed in our laboratory the photovoltaic effect is obtained in the p^+-n-n′-n^+ GaAs structure.

2. Fabrication and characteristics of the photovoltaic GaAs detector

The epitaxial p^+-n-n'-n^+ GaAs structures were grown by vapor-phase epitaxy (VPE), on Si-doped n^+ -GaAs(l00) substrates (n = $10^{18}cm^3$), 2" diameter and 500 (μm thick. There were two basic problems solved by the fabrication of those structures: (i) growth of high-resistant n-GaAs epitaxial layers of maximum thickness and (ii) creation of the depletion region all over this thickness. The growth of thick gallium arsenide epitaxial layers by VPE is complicated by low growth rates and by the imperfections on the surface of the growing layer, such as piramides of growth. For the epitaxial layer growth we have used the technology permitting to obtain n-GaAs epitaxial layer with low concentration of EL-2 defects.

The epitaxial structure consists of three epitaxial layers: p^+ -GaAs top layer with a thickness of 1-2 μm and p ≈ $10^{18}cm^{-3}$, n-GaAs epitaxial layer with a thickness of 60-100 (μm and 10^{11}-$10^{13}cm^{-3}$ and n'-GaAs buffer layer with a thickness of 2-3 μm and n′≈ 5 x $10^{17}cm^{-3}$. The ohmic contacts were prepared by vacuum deposition of Al/Cr and Ni/Ga/Au thin films on the front and rear surface of the structure, respectively.

Investigations of the I-V characteristics of the photovoltaic X-ray detector have shown that those characteristics are similar to that of the conventional solar cells. The behavior of the reverse branch of I- V characteristic i0 (reverse saturation current) is of special importance, because it determines the detector dark current. Under illumination of the photovoltaic X-ray detector by X-rays its I-V characteristics are shifted along the current axis. The typical I-V characteristic of the photovoltaic X-ray detector without illumination is shown in Fig. 1. The small disturbance at approximately -3 V is caused by the fail of measuring system.

The photovoltaic X-ray detector can be used in two operation modes: short circuit mode and open circuit mode. It is preferable to use the detector in short circuit operation mode because, then the response of the detector varies linearly with the X-ray intensity, while the response of the detector in the open circuit mode varies logarithmically.

When the photovoltaic X-ray detector is illuminated, a short circuit current, isc, is generated in the n-GaAs epitaxial layer and the I- V characteristics are shifted along the current axis. The current generated in an ideal photovoltaic detector can be written as

$$i_{sc} = N_g q,$$

where q is electron charge, Ng is the incident flux of all X-ray photons with the energy greater than the bandgap E_g upon the device. For GaAs E_g = 1.424 eV. Fig. 2 shows the short circuit current as a function of incident X-ray doze. One can see that the short circuit current varies linearly with the X-ray doze.

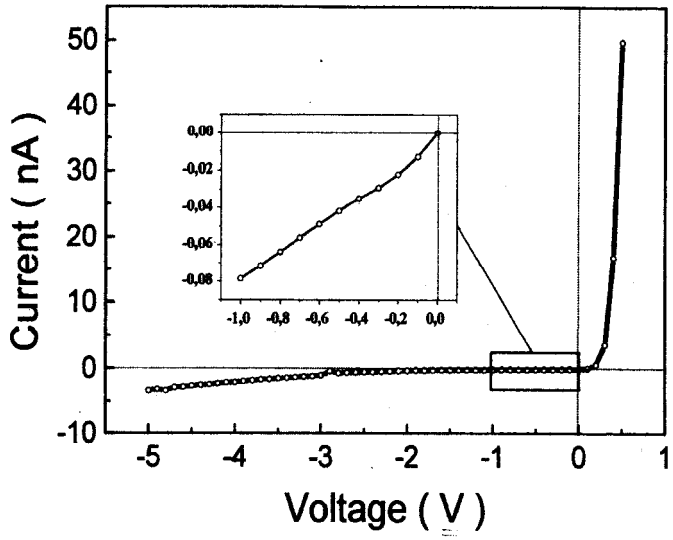

Fig. 1. Typical I-V characteristic of photovoltaic X-ray detector.

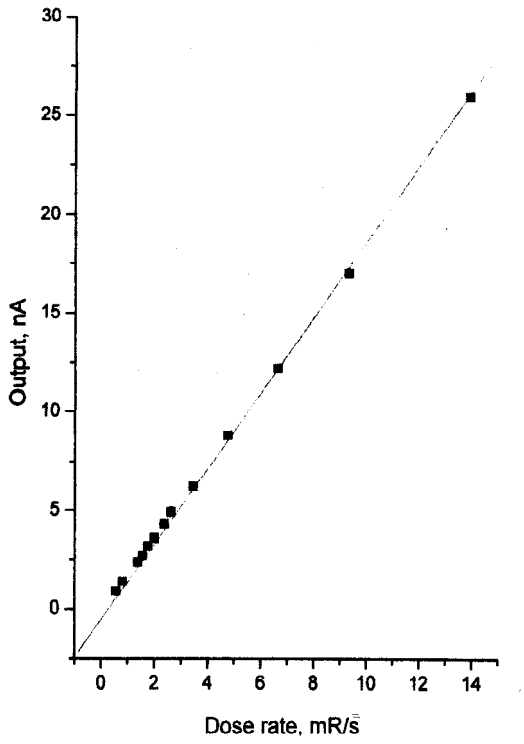

Fig. 2. Short-circuit current of X-ray detector as a function of X-ray dose rate.

The investigation of C-V characteristics has allowed us to control the depletion region in the epitaxial n-GaAs layer, to evaluate the carrier concentration $n = N_d - N_a$ (N_d is a donor concentration, N_a is a acceptor concentration), to spot the profile of the built-in electric field in the depletion region and, at last, to spot the energetic diagram for GaAs(p^+-n-n'-n^+) photovoltaic detector.

Fig. 3 shows the typical C-V characteristic of the photovoltaic X-ray detector. It can be seen that the capacitance is almost constant for reverse and forward biases up to 0.4 V. It is reasonable, therefore, to suppose that the depletion region extends over all the metallurgical thickness of the high resistant n-GaAs epitaxial layer. The presence of the depletion region over the entire thickness of a high-resistant n-GaAs is very important because it gives a opportunity to reduce the the long "tales" of the detector signal due to the carrier generation in the regions where the built-in electric field is neat zero.

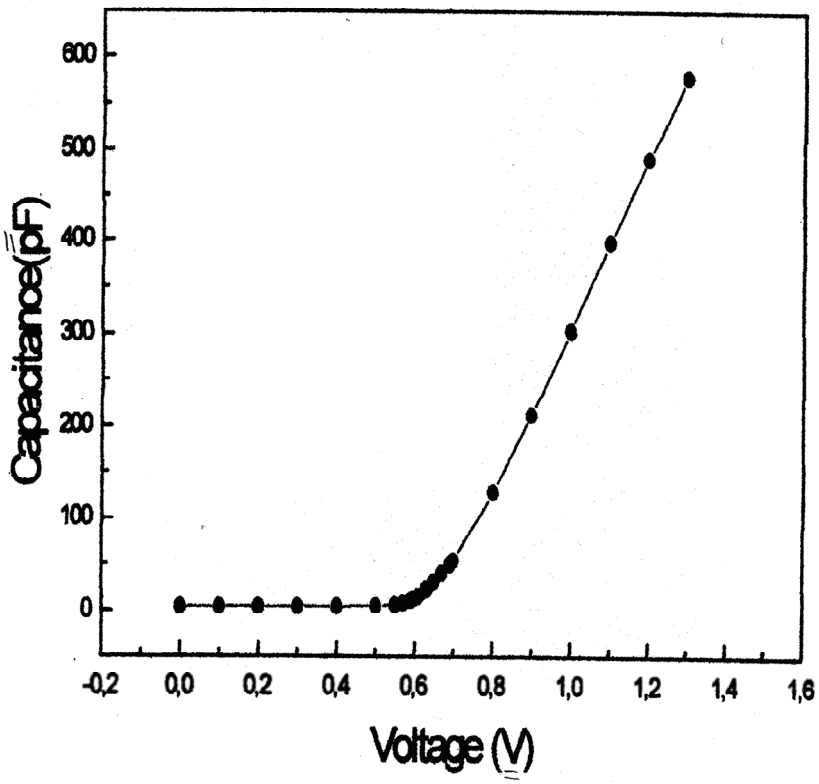

Fig. 3. Typical C-V characteristic of photovoltaic X-ray detector.

A high performance photovoltaic detector must efficiently collect the carriers generated. Maximum detector signal is obtained only when both electrons and holes created by x-ray irradiation in the depletion region are fully collected.

The charge collection efficiency is determined by the thickness of the depletion region and the collection length

$$L_c=(\mu_n\tau_n+\mu_p\tau_p)\cdot E\ ,$$

where μ_n and μ_p are electron and hole mobilities, τ_n and τ_p are electron and hole lifetimes, E is built-in electric field in the depletion region. The lifetime of excess free charge carriers produced by x-ray irradiation in the depletion region is an important parameter for the high charge collection efficiency. Poor collection efficiency is caused by deep level traps which reduce the mobility-lifetime product in GaAs layer. Generally large mobility-lifetime product and high resistivity are required for good transport characteristics resulting in high charge collection efficiency. The long lifetimes (of order of 200 ns) in epitaxial GaAs were obtained by decreasing of EL-2 center concentration to less as 10^{13} cm^{-3} in the *n*-GaAs epitaxial layer.

It should be noted that the carrier collection length decreases if forward bias voltage is applied to photovoltaic detector and transport of carriers via diffusion dominates as detector approaches the open-circuit mode. Let us now consider briefly the role of the depletion region. The concentrations of impurities and charge carriers out of the depletion region are balanced also charge density it is equal to zero. The depletion region almost doesn't contain mobile charges therefore there is here the large gradient of electric field due to the charges of ionized impurities. The thickness of a depletion region is given by

$$W=\left[\frac{\varepsilon}{2\pi e}\left(\frac{1}{N_A}+\frac{1}{N_B}\right)\left(V+\Phi_B\right)\right]^{-1/2},$$

where ε is the dielectric constant, e is the charge of an electron, N_A and N_B are concentrations of acceptors and donors in the p^+ and n layers of the structure, V is the applied voltage and Φ_B is the built-in voltage of the junction. The width of the depletion region can be controlled by the epitaxial technique used to prepare GaAs p^+-n-$n^{\prime}$-n^+ structure or by the application of reverse bias to the junction. Electron-hole pairs generated in the depletion region are separated and accelerated by the built-in electric field and enter the region where they are the majority carriers. Charge carriers generated out of the depletion region but on distance of the mean diffusion length from it will diffuse into the depletion region and drift there. The charge collection efficiency is the most important factor in detector operation. It is defined by three factors, namely by the charge carriers mobility's, by the charge carriers lifetimes and by the electric field in the p-n junction.

The built-in electric field is the origin of photocurrent in the photovoltaic X-ray detector. In order to obtain a reasonable built-in electric field in the depletion region it is important to control accurately the total number of impurities. Direct measurements of the built-in electric field by the EBIC method were made to determine its profile in the epitaxial GaAs (p^+-n-n′-n^+) structure. The junction structure was investigated by the use of Philips SEM 515 scanning electron microscope. In the built-in electric field profile studies the electron beam is incident normal to the edge of epitaxial structure. The profile of built-in electric field in epitaxial GaAs (p^+-n-n′-n^+) structure with depletion region of 80 μm thickness is shown in Fig. 4. One can see here that the built-in electric field exists over the entire epitaxial n-GaAs layer.

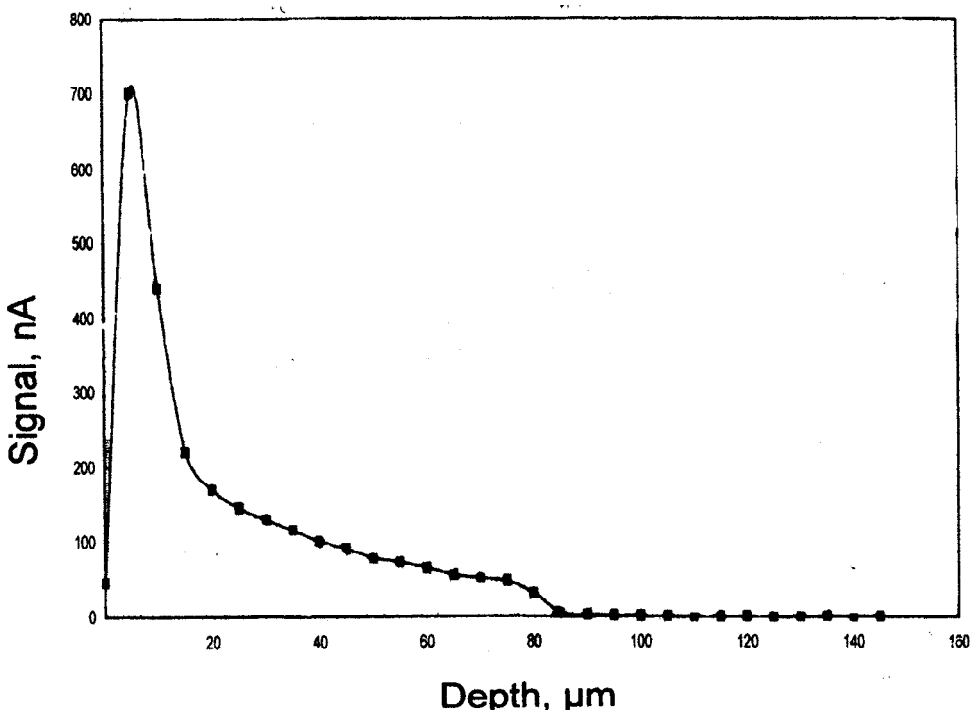

Fig. 4. Profile of the built-in electric field.

The response of the epitaxial GaAs (p^+-n-n′-n^+) detector to charged particles was investigated by the use of α-particles from radioisotope source. We have measured the charge collection efficiency and energy resolution.All measurements were made at room temperature. Registration of α-particles was performed at atmospheric pressure and in vacuum ($p \approx 10^{-4}$Torr) at 0 and 17 V bias voltages. Epitaxial GaAs (p^+-n-n′-n^+) detectors were tested by α-particles from a three-component source U^{233}[4824 keV]-Pu^{238}[5499 keV]-Pu^{239}[5156 keV]. The summary of the results is shown in table 1.

Here Vbias is the bias voltage, Eα(keV) is the energy of the α-particles, Qtheor(e) is the theoretical charge in the detector (in thousands of electron-hole pairs), N(Ch) is the position of peak in ADC counts, σ of the peak is also in ADC counts, Qcol is the measured charge collected in detector and CCE is the charge collection efficiency. The energy resolution better than 1% is obtained at air pressure. One can see on the Table that the charge collection efficiency at zero bias voltage is lower than at 17 V bias. Since the high concentration of electron-hole pairs created by α-particles disturbs significantly the built-in electric field, the electron-hole pairs are not fully collected without a bias voltage.

A photovoltaic X-ray detector was irradiated with ^{241}Am(60 keV) photons. Measurements of the charge collection efficiency obtained with bias voltages of 0 and 17 V show charge collection efficiency of 93.4% and 93.6%, respectively. In this case, the charge collection efficiencies without bias voltage and with the bias of 17 V are the same.

	E_α(keV)	Q_{theor}	N (Ch)	σ (Ch)	Q_{col}	CCE (%)	σ(e)
E_{bias}=0 V P = 740 mmHg	4824	1148.571	317	9.92	873.165	76.0	17.3
	5156	1227.619	375	9.08	974.375	79.4 ,	15.8
	5499	1309.286	431	7.72	1072.095	81.9	13.5
E_{bias}= 17 V P = 740 mmHg	4824	1148.571	378	9.4	979.61	85.3	16.4
	5156	1227.619	448	7.98	1101.76	89.7	13.9
	5499	1309.286	515	7.9	1218.675	93.1	13.8
E_{bias}=0 V P = 0 mmHg	4824	1148.571	519	9.22	905.655	78.9	16.1
	5156	1227.619	561	8.69	978.945	79.7	15.2
	5499	1309.286	599	7.1	1045.255	79.8	12.4
E_{bias} = 17 V P = 0 mmHg	4824	1148.571	622	5.1	1085.39	94.5	8.9
	5156	1227.619	675	4.71	1177.875	95.9	8.2
	5499	1309.286	729	5.2	1272.105	97.2	9.1

Table 1. The summary of α-particle measurements.

The quantum efficiency of the photovoltaic X-ray GaAs detector is limited by the thickness of the n-GaAs layer in the epitaxial structure. The use of a grazing incident angle geometry, which provides a larger absorption length for X-ray photons without increasing the actual thickness of the epitaxial layer, is the only way to increase the quantum efficiency of the photovoltaic GaAs X- ray detector. We have measured the sensitivity of the photovoltaic GaAs detector as a function of effective energy in the range 7-120 keV. The sesitibity S was calculated as

$$S = \frac{I_{ph}}{DA},$$

where I_{ph} is the photocurrent, D is the X-ray dose and A is the sensitive surface area of the detector. The results are shown in Fig. 5. The function has a maximum at 35 keV. The mean sensitivityat this energy was about 30 μA·min/Gy·cm2. Above 35 keV, the detector sensitivity decreases but at a lower rate compared to the decrease in X-ray linear absorption coefficient in GaAs. It can probably be explained by the cascade processes in the epitaxial structure.

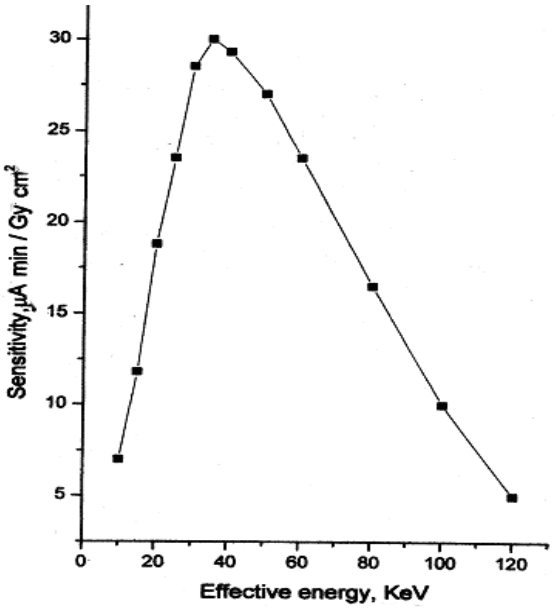

Fig. 5. Sensitivity of the photovoltaic GaAs detector as a function of effective energy.

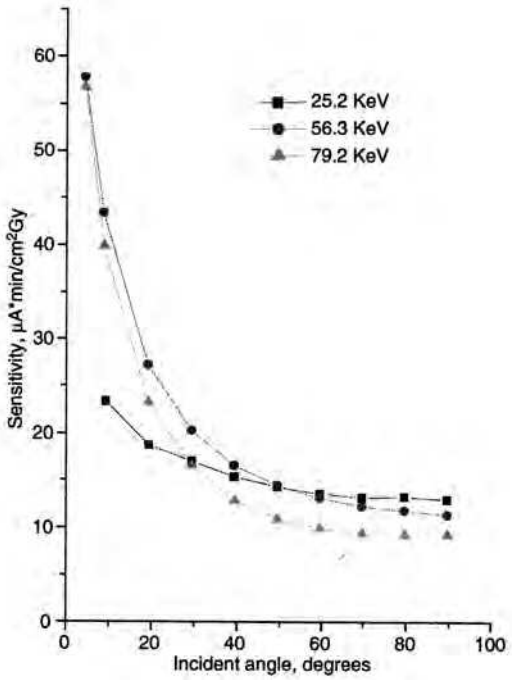

Fig. 6. Sensitivity of the photovoltaic GaAs X-ray detector as a function of the angle.

The quantum efficiency for the photovoltaic GaAs (p^+-n-n′-n^+) detector is limited by the thickness of the n′-GaAs epitaxial layer. To increase the sensitivity of the detector one can use the grazing-incident X-ray photons angle geometry which provides a larger absorption length in the depletion region without increasing the actual thickness. The measured sensitivity as a function of the angle is shown in Fig.6.

3. Multielement X-ray detector made by the use of photolitography

The scribing the channels on the depth greater than 100 μm to separate the pixels in active layer one from another made the linear detector very fragile if we want to decrease pixel size and pitch less than ~ 200 μm. So one cane make the pixel's row by the lithography and separate the pixel's photocurrent with the use of "guard" rings as it is shown in Fig. 7. In our case the pitch was 108 μm.

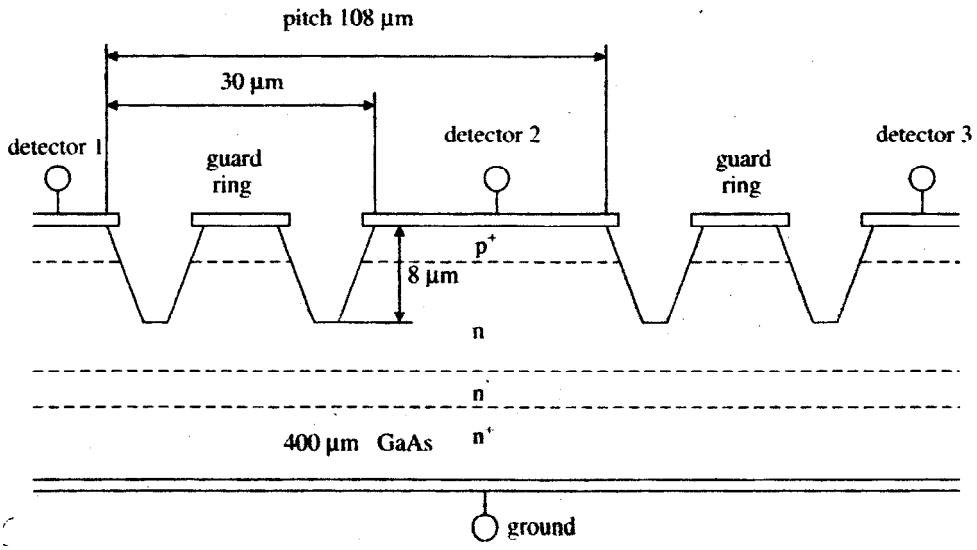

Fig. 7. Intrinsic structure of GaAs (p^+-n-n′-n^+) X-ray detector with guard rings.

In distance of 30 μm between pixels the aluminium conductor of a "guard" ring is located. The "guard" ring is connected to the full- wafer ohmic contact on n^+ side for all detectors (cathode). In p^+ layer and partially in n layer the grooves on depth of 8-10 μm are etched, which separate a conductive p^+ layer between contacts of anodes of detectors and "guard" ring. The anisotropic etch of a solution HCI-$KBr0_3$-H_20 was used with the purpose of decrease of lateral chemical etching of a GaAs material under aluminum contacts. That controlled process carries out the etching on determinate directions of crystallographic planes. The resistance between the nearby contacts is more than $10^6\Omega$. The potential of the full-wafer cathode is formed to suppress interchannel leakages of a photocurrent between anodes of detectors. Signal profiles on the three near-by contacts are shown in Fig. 8.

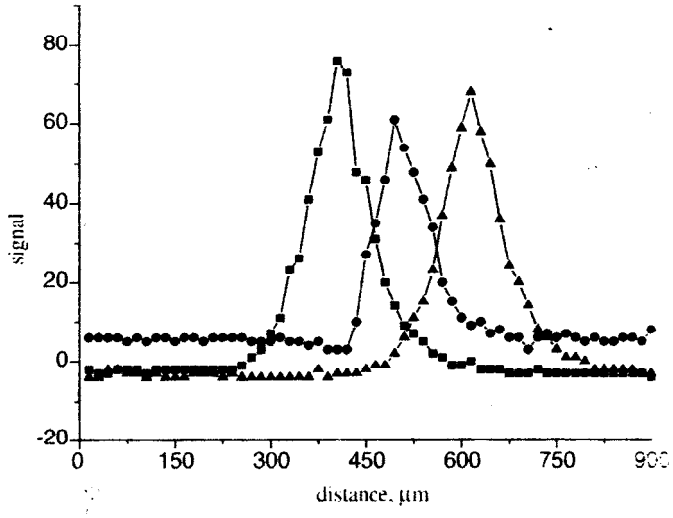

Fig. 8. Signal profiles on the three near-by contacts.

4. Bilinear X-ray detector

In order to increase the spatial resolution of the linear detector one can decrease the pitch and therefore the pixel size. But it leads to decreasing of the signal of the detector. To avoid this one can use a bilinear design of the detector. Let us see the difference between that two types of a detector.

The single or linear multielement detector is a row of pixels (Fig. 9) located along an axis 0X with periodic distance between their geometrical centres: d. The recording of the image is carried out by its scanning in an axis 0Y. The double or bilinear staggered photosensors (Fig. 9b,c) (Bosiers et al, 1995) consist of two rows of linear pixels shifted by one of them in relation to another along an axis OX on the half of pixel's period: d/2, and with distance centre to centre of axes of two rows in d/2. The step of scanning of bilinear row along an axis 0Y is equal d/2. For bilinear row, submitted in Fig. 9 b, the photosensitivity of sensors is lower, as the surface area of the aperture is twice as low as that for viewed here by us (Fig. 9c).

For harmonic intensity modulation in image the appropriate photosensor response, as it is easy to deduce from modulation transfer function (MTF), will correspond to

$$r(f_x, f_y, x, y) = SabMTF(f_x,f_y) \cos[2\pi(f_x x + f_y y)]$$

where S is the detector sensitivity, depending on absorbed photon energy and on detector matter; f_x, f_y are spatial frequencies of the image and a, b are geometrical sizes (apertures) of a rectangle on axes 0X and 0Y (Fig. 9). In a Fig. 10 the dependencies of response difference on value f for rectangular bilinear row with a step $\Delta x = d/2$ and $\Delta y = fy = 0$ for the photosensor moving in space with a step of scanning Δx, Δy, are shown: curve—1 (2a = d), curve—2 (2a/3 = d) and curve—3 (a= d;\ with $\Delta y = b$ and $\Delta x = fy = 0$: curve—1; and linear row: curve —4 ($\Delta x = a = d$, $\Delta y = 0$, $fy = 0$) and ($\Delta y = b = d$, $\Delta x = 0$, $f_x = 0$). For linear row

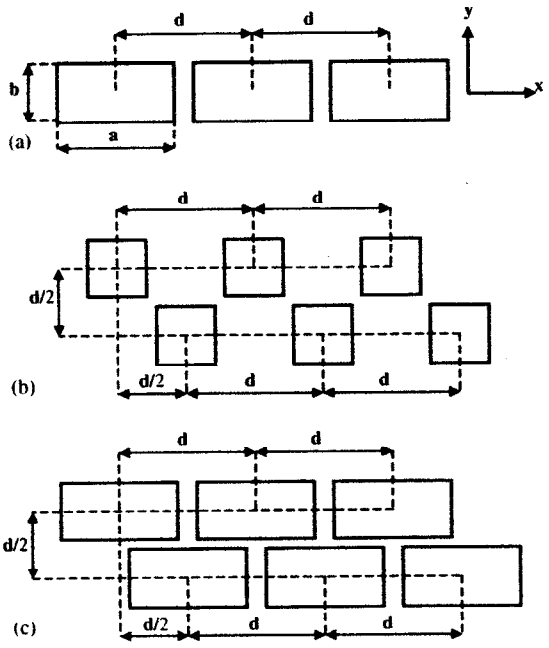

Fig. 9. Kinds of pixel rows.

response difference is higher at low spatial frequencies and lower (worse) at high spatial frequencies, than that for bilinear row. Minimum detectable contrast is evaluated from measurement of the smallest response difference (Munier et al., 1992).

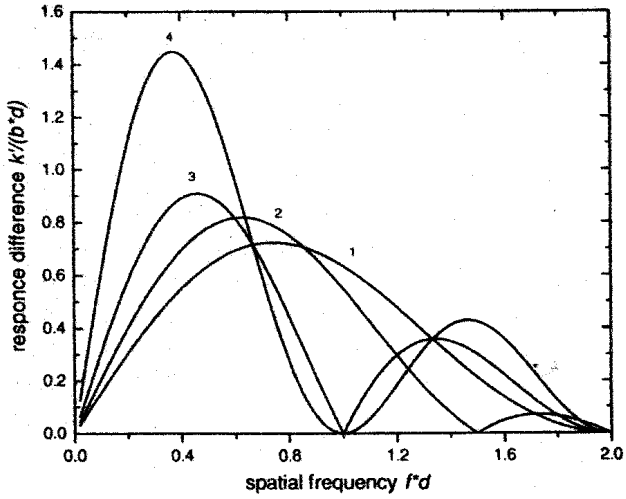

Fig. 10. Dependencies of detector response difference on spatial frequency for bilinear row (1,2,3) and linear row (4).

The multielement detector was made of 2 x 512=1024 pixels with pitch of 0.8 mm in our case. The spatial resolution of double staggered sensor row is twice as high as the resolution of that of single sensor row with the same pitch. Measured spatial resolution is 1.2 line-pairs/mm, contrast sensitivity not worse 1% and dynamic range defined as the ratio of maximum detectable X-ray signal to electronic noise level more than 2000 are received. Read-out operation of detector's signal was realized on near-to-short-circuit mode (Achmadullin et al., 2002). By combining the signal information from two linear rows of detectors a X-ray imaging with improved spatial resolution is received. One can see the X-ray image of fishes as an example of the use of bilinear detector in Fig 11. For comparison in the same figure is placed the image of fish received by the pin-diode detector with a pitch of 200 μm. The image is taken from the paper of G.I. Ayzenshtat et al.,2004. One can see that the noise in the pin-diode image makes the quality of the image much worse.

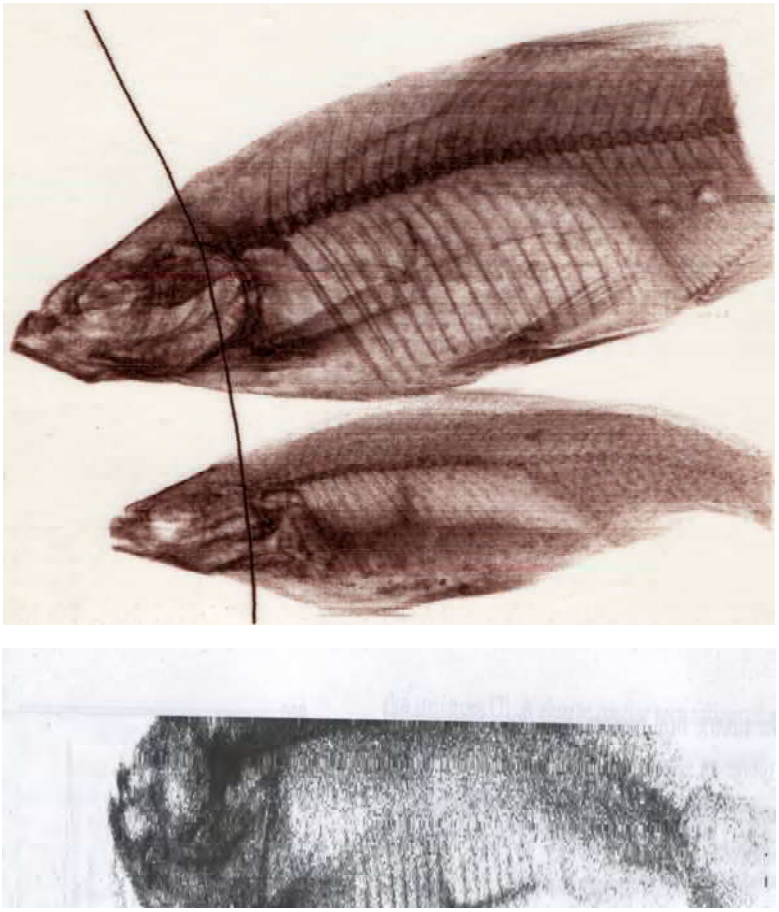

Fig. 11. The X-ray images of fishes. Left image is received by the bilinear detector with 800 μm pitch, right image is received by the pin-diode detector with the 200 μm pitch.

5. Conclusion

We have consicered here the basic features of the GaAs photovoltaic X-ray detector. The detector based on epitaxial p^+-n-n′-n^+ GaAs structures immediately converts X-ray photons to a photocurrent without bias. It has fast response and low noise level. All the measurements described above were made in short-circuit operation mode for the simplicity. To decrease a dose (it is very important in medicine) the detector can operate in pulse-count mode. Photovoltaic GaAs X-ray detectors can find their application in medicine, non-destructive testing, custom houses and other branches.

6. References

Adams R., Bates R., Da Via C., Johnson N.P., O'Shea V., Pickford A., Raine C. and Smith K.. Preliminary results for LP VPE X-ray detectors. *Nuclear Instruments and Methods in Physics Research Section A,* vol.395, Issue 1 (1997), pp. 129-131

Achmadullin R.A., Dvoryankin V.F., Dvoryankina G.G., Dikaev Yu.M., Ermakov M.G., Krikunov A.I., Kudryashov A.A., Petrov A.G., Telegin A.A. Photovoltaic X-ray Detectors Based on Epitaxial GaAs Structures. *Technical Physics Letters*, vol.28, № 1 (2002), pp.15-16

Р.А. Ахмадуллин, В.Ф. Дворянкин, Г.Г. Дворянкина, Ю.М. Дикаев, М.Г. Ермаков, О.Н. Ермакова, А.И. Крикунов, А.А. Кудряшов, А.Г. Петров, А.А. Телегин. Фотовольтаические детекторы рентгеновского излучения на основе эпитаксиальных структур GaAs. *Письма в ЖТФ* (2002), т.28, вып.1, стр. 34-38

Alexiev D., Butcher K.S.A. High purity liquid phase epitaxial gallium arsenide nuclear radiation detector. *Nuclear Instruments and Methods in Physics Research Section A,* vol.317, Issues 1-2 (1992), pp. 111-115

Amendolia C.R., Bertolucci E., Bisogni H.G. Bottigli U., Ciocci M.A., Conti M., Delogu P., Fantacci M.E., Maestro P., Marzulli V., Pernigotti E., Romeo N., Rosso V., Russo P., Stefanini A., Stumbo S. GaAs detector optimization for different medical imaging applications. *Nuclear Instruments and Methods in Physics Research Section A,* vol.434, Issue 1 (1999), pp. 14-17

Ayzenshtat G.I., Germogenov V.P., Guschin S.M., Okaevich L.S., Shmakov O.G., Tolbanov O.P., Vorobiev A.P. X-ray and γ-ray detectors based on GaAs epitaxial strictures. *Nuclear Instruments and Methods in Physics Research Section A,* vol.531, Issue 1 (2004), pp. 97-102

Bates R.L., Manopoulos S., Mathieson K., Meikle A., O'Shea V., Raine C., Smith K.M., Watt J., Whitehill C., Pospsil S., Wilhelm I., Dolezal Z., Juergensen H., Heuken M. Development of low-pressure vapour-phase epitaxial GaAs for medical imaging. *Nuclear Instruments and Methods in Physics Research Section A,* vol.434, Issue 1 (1999), pp. 1-13

Bates R., Campbell M., Cantatore E., D'Auria S., DaVià C., del Papa C., Heijne E.M., Middelkamp P., O'Shea V., Raine C., Ropotar I., Scharfetter L., Smith K. and Snoeys W. Gallium arsenide pixel detectors. *Nuclear Instruments and Methods in Physics Research Section A,* vol.410, Issue 1 (1998), pp. 6-11

Buttar C.M. GaAs detectors - a review. *Nuclear Instruments and Methods in Physics Research Section A,* vol.395, Issue 1 (1997), pp. 1-8

Bencivelli W., Bertolucci E, Bottigli U., Cola A., Fantacci M.E., Rizzo P., Rosso V. and Stefanini A. Electrical characterization and detector performances of a LPE GaAs detector for X-ray digital radiography. *Nuclear Instruments and Methods in Physics Research Section A,* vol.410, Issues 1-2 (1998), pp. 372-376

Bosiers J., Vermeiren J., Sevenhans J. High resolution linear arrays. *Proc. SPIE,* vol. 591 (1995), pp. 67-70

Jenny D.A., Loferski J.J., Rappoport P. Photovoltaic Effect in GaAs Junctions and Solar Energy Conversion. *Phys. Rev.,* vol.101, p.1208, 1956

McGregor D.S., Hermon H., Room-temperature compound semiconductor radiation detectors. *Nuclear Instruments and Methods in Physics Research Section A,* vol.395, Issue 1 (1997), pp. 101-124

Moizhes B.Ya. On the Theory of Photocells with a p-n Junction. *Soviet Physics- Solid State,* vol.2, №2, p.202, 1960

Munier B., Prieur-Drevon P., Roziere G., Ghabbal J. High resolution digital x-ray imaging with solid state linear detectors. *Proc. SPIE,* vol. 1651 (1992), pp. 106-115

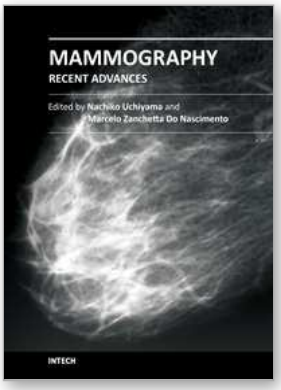

Mammography - Recent Advances
Edited by Dr. Nachiko Uchiyama

ISBN 978-953-51-0285-4
Hard cover, 418 pages
Publisher InTech
Published online 16, March, 2012
Published in print edition March, 2012

In this volume, the topics are constructed from a variety of contents: the bases of mammography systems, optimization of screening mammography with reference to evidence-based research, new technologies of image acquisition and its surrounding systems, and case reports with reference to up-to-date multimodality images of breast cancer. Mammography has been lagged in the transition to digital imaging systems because of the necessity of high resolution for diagnosis. However, in the past ten years, technical improvement has resolved the difficulties and boosted new diagnostic systems. We hope that the reader will learn the essentials of mammography and will be forward-looking for the new technologies. We want to express our sincere gratitude and appreciation?to all the co-authors who have contributed their work to this volume.

INTECH
open science | open minds

InTech Europe
University Campus STeP Ri
Slavka Krautzeka 83/A
51000 Rijeka, Croatia
Phone: +385 (51) 770 447
Fax: +385 (51) 686 166
www.intechopen.com

InTech China
Unit 405, Office Block, Hotel Equatorial Shanghai
No.65, Yan An Road (West), Shanghai, 200040, China
中国上海市延安西路65号上海国际贵都大饭店办公楼405单元
Phone: +86-21-62489820
Fax: +86-21-62489821